Published in final edited form as:
J Phys Chem B. 2012 November 26; 116(46): 13585–13596. doi:10.1021/jp3005794.

A Timesaving Strategy for MAS NMR Spectroscopy by Combining Non-Uniform Sampling and Paramagnetic Relaxation Assisted Condensed Data Collection

Shangjin Sun[1,2,$], **Si Yan**[1,$], **Changmiao Guo**[1], **Mingyue Li**[1], **Jeffrey C. Hoch**[3], **John C. Williams**[4], and **Tatyana Polenova**[1,*]

[1]Department of Chemistry and Biochemistry, University of Delaware, Newark, DE 19716, United States

[3]Department of Molecular, Microbial, and Structural Biology, University of Connecticut Health Center, 263 Farmington Avenue, Farmington, CT 06030-3305, United States

[4]Department of Molecular Medicine, Beckman Research Institute of City of Hope, 1500 East Duarte Road, Duarte, CA 91010, United States

Abstract

We present a timesaving strategy for acquiring 3D magic angle spinning NMR spectra for chemical shift assignments in proteins and protein assemblies in the solid state. By simultaneous application of non-uniform sampling (NUS) and paramagnetic-relaxation-assisted condensed data collection (PACC), we can attain 16-fold time reduction in the 3D experiments without sacrificing the signal-to-noise ratio or the resolution. We demonstrate that with appropriate concentration of paramagnetic dopant introduced into the sample the overwhelming majority of chemical shifts are not perturbed, with the exception of a limited number of shifts corresponding to residues located at the surface of the protein, which exhibit small perturbations. This approach enables multi-dimensional MAS spectroscopy in samples of intrinsically low sensitivity and/or high spectral congestion where traditional experiments fail, and is especially beneficial for structural and dynamics studies of large proteins and protein assemblies.

Keywords

solid-state NMR; magic angle spinning; MAS; PACC, non-uniform-sampling

[*]To whom the correspondence should be addressed: Tatyana Polenova, Department of Chemistry and Biochemistry, University of Delaware, Newark, DE 19716, tpolenov@udel.edu, Tel. (302) 831-1968, FAX (302) 831-6335.
[2]Current address: Structural Biophysics Laboratory, Center for Cancer Research, National Cancer Institute, Frederick, MD
[$]These authors contributed equally to this publication

SUPPORTING INFORMATION

Figures with i) ^{1}H T1 and ^{15}N T2* relaxation curves for neat LC8 and LC8 doped with Cu(II)-EDTA of various concentrations; ii) chemical shift deviations in 3D NCACB spectra recorded by NUS-PACC in LC8 doped with Cu(II)-EDTA at 5, 10, and 50 mM with respect to those recorded by US in neat LC8; iii) backbone torsion angles Ψ and Φ derived by TALOS+ using the chemical shifts of LC8 doped with 5 mM Cu(II)-EDTA recorded in NUS-PACC experiments; iv) 2D planes of 3D NCOCA NUS-PACC spectrum processed with MaxEnt and MDD. Tables with solution and solid-state chemical shift perturbations of LC8 for various Cu(II)-EDTA dopant concentrations, solid-state chemical shifts for LC8 doped with 5 mM Cu(II)-EDTA, chemical shift differences in a pair of 3D NCACB spectra (NUS and US) for LC8 doped with 5 mM Cu(II)-EDTA, the chemical shift assignments for the LC8 with 5 mM Cu(II)-EDTA by 3D NUS NCACB, NCACO and NCOCA spectra, standard deviations for the resolved residues in 3D NUS-PACC NCOCA spectra acquired three times, and the NUS schedules for the 3D experiments. This material is available free of charge via the Internet at http://pubs.acs.org.

INTRODUCTION

Magic angle spinning (MAS) solid-state NMR spectroscopy is an emerging structural biology technique and is unique among other methods as it can provide atomic-level structure and dynamics information in biological systems that are very large, insoluble and lack long-range order, and thus not amenable to X-ray crystallography or solution NMR spectroscopy.[1–9] Most of the protocols for extracting structural or dynamics information by NMR require site-specific chemical shift assignments as the initial step.[10–12] Resonance assignments by MAS NMR require acquisition of a set of homonuclear and heteronuclear multidimensional (typically 3D) spectra to establish internuclear (intra-residue and sequential) connectivities in order to identify the amino acid type and its position in the polypeptide chain.[13,14] These multidimensional spectra must have adequate sensitivity and resolution in order to enable reliable resonance assignments.[15] Both requirements in turn often translate into long experiment times, for instance when the NMR samples are of intrinsically low sensitivity and/or high chemical shift degeneracy, such as in proteins and protein assemblies of high molecular weight and/or in isotopically dilute samples. Such long experimental times are generally impractical for a number of reasons, such as sample and/or instrument instability, and general instrument time constraints. Timesaving strategies are therefore highly desirable in multidimensional MAS NMR spectroscopy, as they would expand the range of biological systems amenable to detailed structural and dynamics analysis.

Among the methods developed with the goal of reducing the experiment time in the MAS NMR measurements, Paramagnetic-relaxation-Assisted Condensed data Collection (PACC) introduced by Ishii and coworkers permits 5–20 fold timesaving by decreasing the recycle delay.[16] This approach requires i) paramagnetic doping (typically by Cu(II)-EDTA) of the protein samples resulting in the reduced ^{1}H longitudinal relaxation time and ii) very fast MAS frequencies (40 kHz or higher) allowing for low-power proton decoupling during RF pulses and acquisition time. Similar approaches have been applied to protein systems that have natural metal centers or artificially introduced paramagnetic tags.[17–21] Recently, Jaroniec and coworkers extended the PACC approach to 3D experiments for resonance assignment as well as for acquiring distance restraints.[21] An apparent advantage of these paramagnetic-relaxation-assisted approaches is that no major hardware upgrades are required except for a need to have a fast MAS probe capable of rotation frequencies of at least 40 kHz.

Another unexplored advantage of PACC is that it can be applied in conjunction with other timesaving strategies such as non-uniform sampling (NUS) protocols[22–26], which would result in further significant reductions in experiment time. An experiment otherwise occurring in the “sensitivity-limited regime” can be brought into the “sampling-limited regime”[27] when PACC is applied. In the “sampling-limited regime”, many sparse sampling techniques have been introduced to save time in multidimensional NMR experiments by omitting acquisition of some FIDs[24–26]. Recently, we have demonstrated that in biological solids, NUS data collection gives rise to large sensitivity enhancements (ca. two-fold in each indirect dimension) when random exponentially biased sampling schedules are used,[28] and these signal enhancements originate in the time domain as was shown previously.[29] Time-domain signals acquired non-uniformly require processing algorithms other than conventional Discrete Fourier Transform (DFT). For example, radial sampling requires the time domain signal to be processed with G-matrix Fourier transform[15], projection reconstruction[30], automated projection spectroscopy (APSY),[31] projection decomposition (PRODECOMP)[32] or high resolution iterative frequency identification for NMR (HIFI-NMR). [33] Random non-uniformly sampled data can be processed with maximum entropy reconstruction,[24] multidimensional decomposition (MDD),[34] forward maximum entropy

reconstruction (FM),[35] l_1-norm regularization (also called compressed sensing),[36–38] Spectroscopy by Integration of Frequency and Time domain information (SIFT),[39] non-uniform Fourier transformation (NU-FT),[40] and Gridding-FFT (GFFT)[41]. Recently, we have introduced a Maximum Entropy Interpolation (MINT) processing protocol that attains full linearity between the time and the frequency domains and permits direct analysis of the frequency-domain spectra acquired by NUS with respect to those recorded by the conventional uniform sampling (US) protocol. With NUS/MINT we have demonstrated that inherent properties of solid-state signals (relatively short T_2*) permit collection of datasets possessing both enhanced sensitivity and retained resolution.[28]

To the best of our knowledge, the above non-Cartesian sampling techniques in conjunction with nonlinear data processing protocols to date have only occasionally been applied in solid-state NMR spectroscopy,[42–45] despite their excellent potential to facilitate data acquisition without compromising on the spectral quality. We expect that the introduction of new techniques for sensitivity and resolution enhancement in solid-state NMR spectroscopy (e.g. dynamic nuclear polarization (DNP),[46] paramagnetic-relaxation-assisted condensed data collection (PACC),[16] In-Phase-Anti-Phase spectroscopy (IPAP),[47] and Spin-State-Selective Excitation (S^3E)[48]) will make the applications of non-uniform sampling techniques more widespread.

In this report, we present a timesaving strategy dubbed NUS-PACC for acquiring 3D MAS solid-state NMR spectra, which is based on the simultaneous use of PACC[16] and random exponentially biased non-uniform sampling (NUS) in the indirect dimensions. We adopted this approach in order to be able to work with sensitivity-limited samples, such as assemblies of U-^{13}C,^{15}N-enriched microtubule-associated proteins in complex with natural abundance microtubules[8] and sparsely U-^{13}C,^{15}N- (amino-acid specifically) enriched assemblies of HIV-1 capsid proteins,[9] where we hit severe sensitivity limitations preventing us from collecting heteronuclear 3D MAS NMR spectra for resonance assignments and/or structure determination. Using this NUS-PACC method, we demonstrate that at least 16-fold timesaving is attained in each of three 3D experiments, NCOCA, NCACO and NCACB, which are key experiments for resonance assignments of proteins and protein assemblies by MAS NMR. We discuss the sample and the experimental conditions required for accurate measurements of the chemical shifts. The approach demonstrated in our work is expected to be generally beneficial for samples of intrinsically low sensitivity and high spectral congestion.

EXPERIMENTS AND METHODS

Expression and purification of isotopically enriched LC8

Expression and purification of U-^{15}N and U-^{15}N,^{13}C isotopically enriched dynein light chain LC8 was reported by us previously. [49]

Preparation of solution and solid-state NMR samples of U-15N and U-15N,13C LC8 doped with Cu(II)-EDTA

For the preparation of solution NMR sample, 500 ul of 10 mg/ml LC8 solutions different Cu(II)-EDTA concentrations (0 mM, 5 mM, 10 mM, 20 mM, and 50 mM) with 10% D_2O were placed into solution NMR tubes. For the preparation of solid-state NMR samples, U-^{15}N or U-^{13}C,^{15}N enriched purified LC8 solutions were dialyzed against 10 mM MES buffer (10 mM $MgCl_2$, pH 6.0) and concentrated to 30 and 25 mg/ml, respectively. The 1M Cu(II)-EDTA stock solution (dissolved in 10 mM MES buffer described above) was added to the concentrated U-^{15}N LC8 solution and to the 32% w/v solution of PEG-3350 (also dissolved in 10 mM MES buffer) in several aliquots to reach the final concentration of

Cu(II)-EDTA in the protein and PEG-3350 solutions of 5 mM, 10 mM, 20 mM, and 50 mM. The above PEG-3350 solutions containing Cu(II)-EDTA at desired concentrations were gradually added to the solutions of LC8 containing the same Cu(II)-EDTA concentrations to generate protein precipitates, following the controlled precipitation protocol.[50] A control LC8 sample containing no Cu(II)-EDTA was also prepared. The solid-state samples of LC8 containing different concentrations of Cu(II)-EDTA (0 mM, 5 mM, 10 mM, 20mM and 50 mM) were packed into 3.2, 1.8, or 1.6 mm MAS rotors for subsequent NUS-PACC or conventional experiments. The final amounts of protein precipitate packed in a rotor ranged from 4.8 to 15 mg, depending on the rotor size.

Solid-state NMR spectroscopy

Magic angle spinning solid-state NMR spectra of the U-^{15}N and U-^{13}C,^{15}N labeled LC8 samples containing different concentration of the paramagnetic dopant were acquired at 14.1 T (600 MHz) on a narrow bore Varian InfinityPlus instrument outfitted with three probes: i) a 3.2 mm triple resonance Varian T3 probe; ii) a 1.8 mm triple resonance fast-MAS probe developed and built in the laboratory of our collaborator, Dr. Ago Samoson (Technical University of Tallinn); and iii) a 1.6 mm triple resonance fast-MAS Varian probe. Larmor frequencies are 599.5 MHz for ^{1}H, 150.7 MHz for ^{13}C, and 60.7 MHz for 15N. The experiments were conducted at the MAS frequencies of 10±0.001 or 40±0.001 kHz controlled by a Varian MAS controller. The temperature was calibrated for each probe at different MAS frequencies using either a $PbNO_3$ [51] or KBr52 temperature sensor, and the actual temperature at the sample was maintained to within ±1 °C throughout the experiments using the Varian temperature controller. The NMR experiments were carried out at the following temperatures: i) for 10 kHz MAS frequency, T = −16.7 °C (apparent temperature of −20 °C); ii) for 40 kHz MAS frequency, T = −15 °C (apparent temperature of −35 °C). 1H, ^{13}C and ^{15}N chemical shifts were referenced with respect to DSS, adamantane and ammonium chloride used as external referencing standards.[53]

^{1}H T_1 and ^{15}N T_2 measurements—^{1}H T_1 and ^{15}N T_2 of Cu(II)-EDTA doped U-15N LC8 samples were measured at 10 kHz with ^{15}N CP-based inversion recovery and spin-echo experiments, respectively.[54] ^{1}H T_1 and ^{15}N T_2 of U-^{13}C, ^{15}N Cu(II)-EDTA doped LC8 samples were measured according to the same procedures as for ^{15}N enriched LC8 (*vide supra*), at MAS frequencies of 10 and 40 kHz.

NUS-PACC experiments on Cu(II)-EDTA-doped LC8—The typical 90-degree pulse lengths were 2.7 μs (^{1}H) and 4.17 μs (^{13}C). The ^{1}H-^{15}N cross polarization radio frequency fields were set to $\omega H + \omega_{N(center)} = \omega_{MAS}$ with a linear ramp on ω_N (center at 10 kHz). ^{15}N-^{13}C DCP/SPECIFIC-CP[55,56] radio frequency fields were set to $\omega_N + \omega_{C(center)} = \omega_{MAS}$ with tangential ramp on ω_C (center at 20 kHz).[18] 10 kHz low-power TPPM[57,58] decoupling was used during the acquisition and evolution periods in the indirect dimensions. RFDR[59,60] or DREAM[61] homonuclear magnetization transfer schemes were used following the DCP step to acquire NCACX, NCOCX, NCACB, NCACO or NCOCA spectra (pulse sequences are shown in Figures 1A and 1B). Rotor-synchronized XY-16 sequences (40 kHz π pulse at the center of each rotor period) were applied for RFDR, and the mixing time was 2.4 ms. In the DREAM sequence, tangential ramp centered at 16 kHz with 2.4 ms mixing time was used for C'-C^{α} and C^{α}-C' magnetization transfers; tangential ramp centered at 20 kHz with 2.5 ms mixing time was used for C^{α}-C^{β} magnetization transfer. No proton decoupling was applied during RFDR or DREAM period. For NCACO and NCACB experiments, the ^{13}C carrier frequency was placed at 56.6 ppm; for NCOCA experiment- at 174.6 ppm; no frequency offset was applied in any experiment during the DREAM mixing.

In the non-uniformly sampled 3D experiments (DCP-DREAM-based NCACB, NCACO and NCOCA, the pulse sequence is shown in Figure 1B), four FIDs were acquired in the (RR, IR, RI, II) sequence for each NUS (t_1, t_2) combination, corresponding to a States-States[62] hypercomplex acquisition mode used for phase-sensitive detection in the indirect dimensions. Three random non-uniform sampling schedule (see Figure 2) was created by ScheduleTool (software documentation available at http://sbtools.uchc.edu/nmr/sample_scheduler/).[63] The ^{15}N T_2 * value was used as a guide for constructing the non-uniform sampling schedule for 3D NCOCA, NCACO and NCACB experiments as described.[28] ^{15}N T_2 * was estimated from 1D ^{15}N CPMAS and 2D NCA spectra. For all samples, the NUS schedule contained 25% hypercomplex points with respect to the corresponding US schedule. For the 5 mM Cu(II)-EDTA LC8 sample, 256 hypercomplex NUS points were acquired (the maximum increment in the NUS dataset for both indirect dimensions corresponds to point #32 in the US dataset that would be acquired with the same dwell time) for NCOCA and NCACB experiments, and 192 hypercomplex NUS points were acquired (the maximum increments in the NUS dataset for ^{15}N and ^{13}C indirect dimensions correspond to points #32 and #24, respectively, in the corresponding US dataset that would be acquired with the same dwell time) for NCACO. The total experiment times are 9 hours for NCOCA (64 scans), 14 hours for NCACO (128 scans) and 27 hours for NCACB (192 scans). To evaluate the effects of NUS on chemical shift deviation, two US NCACB experiments were carried out with experimental settings identical as those in the NUS-PACC NCACB experiment except that the evolution times in the indirect dimensions were sequentially incremented, and the final number of points collected in the indirect ^{15}N and ^{13}C dimensions were 32×32 (experiment 1) and 16×12 (experiment 2). For the 10 mM Cu(II)-EDTA LC8 sample, 384 hypercomplex points were acquired (the maximum increments in the NUS dataset for ^{15}N and ^{13}C indirect dimensions correspond to points #32 and #48, respectively, in the corresponding US dataset that would be acquired with the same dwell time). The total experiment time is 54 hours for NCACB (256 scans). For the 50 mM Cu(II)-EDTA LC8 sample, 324 hypercomplex points were acquired (the maximum increment for both indirect dimensions corresponds to point #36 in the US dataset that would be acquired with the same dwell time).

Conventional US/FFT experiments on neat LC8—For the experiments acquired at 40 kHz, the typical 90-degree pulse lengths were 2.7 μs (^{1}H) and 4.17 μs (^{13}C). The ^{1}H-^{15}N cross polarization rf fields were set as $\omega_H - \omega_{N(center)} = \omega_{MAS}$ with a linear ramp on ω_N (center at 55 kHz). ^{15}N-^{13}C DCP/SPECIFIC-CP[55,56] rf fields were set as $\omega_N - \omega_{C(center)} = \omega_{MAS}$ with tangential ramp on ω_C (center at 25 kHz).[18] 10 kHz low-power TPPM[57,58] decoupling was used during the acquisition and indirect-dimension evolution periods. DREAM61 homonuclear magnetization transfer schemes were used following the DCP step to acquire NCACB spectra. In the DREAM sequence, tangential ramp centered at 20 kHz with 1.9 ms mixing time was used for C^{α}-C^{β} magnetization transfer. No decoupling was applied during the DREAM period. States-States[62] hypercomplex acquisition mode was used for phase-sensitive detection in the indirect dimensions. The NCACB spectrum was acquired with 144 scans, 18 complex points in t1 and 18 complex points in t_2.

Solution NMR spectroscopy

^{1}H-^{15}N HSQC spectra of U-^{15}N-LC8 samples containing different concentrations of paramagnetic Cu(II)-EDTA dopant (0 mM, 5 mM, 10 mM, 20mM and 50 mM, see above) were acquired at 14.1 T on a Bruker Avance spectrometer. Larmor frequencies are 600.133 MHz (^{1}H), 60.8 MHz (^{15}N). All experiments were conducted at 298 K. Chemical shifts were referenced to DSS.[64] Additional acquisition and processing parameters are specified in the Supporting Information.

NMR data processing and analysis

The NUS 3D data were converted by in-house written python scripts in conjunction with the bin2pipe module in NMRPipe[65] from the Chemagnetics format to a format in which each data point is in an IEEE float-32 format, whereas those points in the uniform grid omitted by NUS were zero filled, and the real/imaginary parts were interleaved in every dimension.

The converted data were processed with DFT in the direct dimension and with maximum entropy reconstruction in the indirect dimensions as implemented in the program Rowland NMR Toolkit (software documentation available at http://rnmrtk.uchc.edu).[66–68] In the direct dimension, a 90-degree or 60-degree sine bell apodization function was applied to the converted data, followed by Lorentzian-to-Gaussian apodization, zero filling to 1024 points, Fourier transform and phase correction. In the indirect dimensions, the 1024 planes were reconstructed to 128 × 128 2D slices. MINT processing was applied as described.[28]

In parallel, the converted data were also processed with the MDD algorithm.[34] Three software packages were used to implement the MDD data processing: mddNMR,[34] MDDGUI (software courtesy of Cheryl Arrowsmith and Aleksandras Gutmanas) and NMRPipe.[65] In addition, in-house written python scripts were used to aid the conversion of data from the NMRPipe format to the mdd format as our current implementation of NUS in spinsight/Chemagnetics does not generate parameter files (e.g. Bruker acqus, Varian procpar files) that could be parsed by mddNMR and MDDGUI. In the direct dimension, a 60-degree sine bell apodization function was applied to the converted data, followed by Lorentzian-to-Gaussian apodization, zero filling to 1024 points, Fourier transform and phase correction. The resulting interferograms were divided into small regions of interest (ROIs, each ROI is 1.0 ppm and two neighboring ROIs have 0.5 ppm overlap) and converted to mdd format. Each mdd file for a small ROI was subjected to multidimensional decomposition carried by mddNMR in order to reconstruct a full grid interferogram. The full grid interferograms for each ROI were combined and converted back to the NMRPipe format, and the two indirect dimensions were processed by NMRPipe with forward linear prediction of the number of points equal to that in the experimental data, 30, 60 or 90-degree sine bell followed by Lorentzian-to-Gaussian apodization, zero filling, Fourier transform and phase correction.

The conventional uniformly sampled data were processed in rnmrtk (following the MINT protocol, as described in NUS data processing) and in NMRPipe.[65] For the processing by NMRPipe, we applied forward linear prediction in the indirect dimensions of the number of points equal to that in the experimental data; 90-degree or 60-degree sine bell was applied to each dimension followed by Lorentzian-to-Gaussian apodization, zero filling, Fourier transform and phase correction.

The processed spectra were analyzed in Sparky.[69]

RESULTS AND DISCUSSION

Effects of Paramagnetic Doping of Cu(II)-EDTA on ^{1}H T_1 and ^{15}N T_2 of LC8

Under the optimal sample conditions, in the presence of a paramagnetic dopant, the ^{1}H longitudinal relaxation time T_1 should be significantly shortened while the ^{15}N and ^{13}C transverse relaxation times T_2 should be close to those of neat samples. The previous study by Ishii and coworkers demonstrated that the concentration of the paramagnetic dopant has the most dramatic effect on the relaxation times, and that the optimal concentration of the paramagnetic dopant is sample specific.[16] To examine the effect of paramagnetic doping on the protein under study, dynein light chain 8 (LC8), we measured ^{1}H T_1 and ^{15}N T_2 for four U-^{15}N-enriched LC8 samples: neat protein and protein doped with 5, 10, 20, and 50 mM Cu(II)-EDTA. The dopant concentration dependencies of ^{1}H T_1 and ^{15}N T_2 for LC8

measured at the MAS frequencies of 10 kHz are listed in Table 1 and shown in Figure S1 of the Supporting Information). For the LC8 sample doped with 50 mM Cu(II)-EDTA, ^{1}H T_1 dropped to 11.4 % (48 ms) of that for the neat sample (~422 ms) while the ^{15}N T_2 has remained the same as for the neat protein (29 ms for the doped and 23 ms for the neat samples, respectively, shown in Figure S1 of the Supporting Information). Similar measurements were also carried out at the MAS frequency of 40 kHz on U-^{13}C,^{15}N-enriched LC8 (neat sample and samples doped with 5, 10, and 50 mM Cu(II)-EDTA). The trends are consistent with our findings for the U-^{15}N-enriched LC8). The doubly labeled sample has short ^{1}H T_1 and long ^{15}N T_2, and these relaxation times exhibit pronounced concentration dependence (listed in Table 1 and illustrated in Figure S1 and Figure S2). The slightly longer ^{1}H T_1 for the doubly labeled sample is due to the attenuation of the effects of dipolar coupling and chemical shift anisotropy by fast MAS.

On the basis of these results we conclude that at dopant concentrations between 5 and 50 mM relaxation properties are favorable for NUS-PACC experiments.

Effects of Paramagnetic Doping of Cu(II)-EDTA on Solution and Solid-State Chemical Shifts

Dopant-induced chemical shift perturbation in solution—In light of the favorable relaxation properties of Cu-doped LC8 samples making them potentially suitable for NUS-PACC experiments, we turned our attention to the chemical shift perturbation as a function of the dopant concentration. It is well known that when present in proximity to the nucleus of interest, unpaired electrons induce chemical shift perturbations, the extent of which depends on the nature of the paramagnetic site, on the nuclear-electron distance as well as on the experimental parameters.[70] Therefore, we conducted a systematic analysis of paramagnetically induced 15N and 1H shift perturbations in solution to examine the possibility of using HSQC spectra as a way of rapidly screening the dopant concentrations to find the most suitable sample conditions for NUS-PACC experiments. As shown in Table S1 of the Supporting Information, at Cu(II)-EDTA concentrations of 20 and 50 mM, significant number of peaks are shifted, and some peaks are broadened beyond detection. Not surprisingly, these resonances belong to residues located at the termini, loops, and surface of the protein. At lower concentrations of Cu(II)-EDTA, the majority of the chemical shifts are intact. These solution experiments suggest that LC8 samples prepared with 5 and 10 mM Cu(II)-EDTA may be best suited for NUS-PACC experiments.

Dopant-induced chemical shift perturbation in the solid state—We next examined the influence of Cu(II)-EDTA on 13C and 15N solid-state chemical shifts in the 2D MAS NCA and NCACB datasets. In Figure 3, NCA and NCACB spectra are shown for LC8 doped with 5, 10, and 50 mM Cu(II)-EDTA, overlaid onto the spectra of the neat LC8 sample. It is clear that at 5 mM the effect on the spectra is modest with the majority of the peaks not affected by the paramagnetic dopant and only a few resonances exhibiting small chemical shift perturbations. For this sample, the mean chemical shift differences vs. the non-doped protein and the standard deviations in ppm are: 0.12 ± 0.11 (^{15}N) and 0.05 ± 0.05 (^{13}C). In contrast, higher concentrations of the Cu(II)-EDTA dopant (10 and 50 mM) induce significant changes to the spectra including chemical shift perturbations and broadening of peaks. The chemical shift perturbations for individual peaks as a function of the dopant concentration are presented in Table S2 and Figure S3 of the Supporting Information. In Figure 4, the peaks that are either missing or have perturbed chemical shifts are mapped onto the X-ray structure of LC8. Not surprisingly, the peaks affected by the paramagnetic copper are located on the surface of the protein.

Effects of Non-Uniform Sampling and Experimental Conditions on Chemical Shift Accuracy in the Solid State

We next analyzed whether non-uniform sampling of the data points in the indirect dimension(s) may affect the accuracy of the measured frequencies and hence introduce additional artificial chemical shift variations in the 2D and 3D NUS spectra, for the LC8 sample doped with 5 mM Cu(II)-EDTA. The results summarized in Figure 5 and in Table S3 clearly demonstrate that the effects are minor, and for the spectra acquired under similar conditions, with sufficiently long evolution times in the indirect dimensions, the mean standard deviations of the chemical shifts are 0.06 ppm (15N) and 0.04 ppm (^{13}C), respectively. It is noteworthy that the chemical shift differences between NUS and US spectra with relatively longer evolution times are significantly smaller than those between the two US spectra, one of which has short evolution times.

The chemical shift accuracy is critically dependent on maximum evolution times.[67] As illustrated in Figure 5 with a pair of 3D US NCACB spectra of LC8 doped with 5 mM Cu(II)-EDTA, when the evolution times are reduced in the indirect dimensions, large discrepancies in chemical shifts are observed with respect to the dataset acquired with appropriate evolution times. In this case, the mean chemical shift differences and the standard deviations are 0.09 ± 0.09 (^{15}N) and 0.07 ± 0.09 (^{13}C), which are comparable to or even higher than the perturbations introduced by the presence of Cu(II)-EDTA. This indicates the benefits of NUS for improving chemical shift accuracy because it allows sampling data points at longer evolution times otherwise not allowed within the constraints of short experimental time.

Taken together, the above results indicate that the LC8 sample prepared with 5 mM Cu(II)-EDTA is well suited for NUS-PACC experiments aimed at resonance assignments. In this sample, minor chemical shift perturbations occur in a fraction of surface residues. These small perturbations can be readily corrected for by comparison of 2D NCACX and NCOCX spectra of the doped and the neat samples. At the same time, if needed, LC8 samples with higher Cu(II)-EDTA dopant concentration of 10–50 mM possessing shorter T_2* relaxation times can be used for rapid screening of NUS-PACC experimental conditions. Generally speaking, our findings also indicate that sample conditions have to be optimized for each system of interest prior to conducting NUS-PACC experiments to assure the desired relaxation parameters are attained with the minimal possible concentration of paramagnetic dopant so that chemical shifts are intact or minimally perturbed with respect to the non-doped sample.

^{13}C Homonuclear Recoupling in 3D Experiments With Condensed Data Collection at Fast MAS Frequencies

In the typical 3D NCACX or NCOCX experiments, a homonuclear magnetization transfer period is added after the DCP[55] or SPECIFIC-CP[56] step. To allow for condensed data collection, the homonuclear recoupling period must be short and must consist of low-power RF radiation yet it must have high magnetization transfer efficiency under fast MAS conditions. Therefore, first-order recoupling sequences appear to be advantageous for the homonuclear mixing in the NUS-PACC experiments (the drawback is dipolar truncation in these methods precluding the observation of lon-grange correlations). Previous studies[16,19,21] employed RFDR[59,60] or DREAM61 for condensed data collection under fast magic angle spinning. We carried out a series of 1D NCACX (or NCACB, NCACO) and NCOCX (or NCOCA) type experiments on U-^{13}C,^{15}N-enriched LC8 doped with 50 mM Cu(II)-EDTA and compared the homonuclear transfer efficiency during the RFDR and DREAM mixing. Our results demonstrate that DCP-DREAM experiments have higher signal-to-noise ratio than the corresponding DCP-RFDR experiments performed with the

same number of scans (see Table 2; the pulse sequences for DCP-RFDR and DCP-DREAM are shown in Figure 1A and B). The other advantages of DREAM are its short duration (~3–4 ms) and low-power RF radiation (~16 kHz or ~20 kHz on ^{13}C channel), with no proton decoupling required. At the MAS frequency of 40 kHz, DREAM can be used to achieve C'-Cα, Cα-C' and Cα-Cβ homonuclear recoupling by adjusting the RF field strength on the ^{13}C channel according to $n\omega_r = (\omega_{rf}^2 + \Omega_1^2)^{1/2} + (\omega_{rf}^2 + \Omega_2^2)^{1/2}$.[61] Therefore, the same DCP-DREAM sequence can be used for three experiments: NCOCA, NCACO and NCACB. In favorable cases, these three experiments will be sufficient for establishing complete site-specific resonance assignments.

We note after the work on this manuscript has been completed, several classes of efficient homonuclear recoupling sequences suitable for fast-MAS conditions have emerged, first-order[71] and second-order methods.[72,73] These sequences should be well suited for NUS-PACC experiments, and assessment of their utility to resonance assignments and acquisition of tertiary distance restraints is currently ongoing in our laboratory.

Non-Uniformly Sampled 3D Experiments With Condensed Data Collection at MAS Frequency of 40 kHz

We recorded three non-uniformly sampled 3D DCP-DREAM spectra, NCOCA, NCACO and NCACB on U-^{13}C,^{15}N-enriched LC8 doped with 5 mM Cu(II)-EDTA (see Experiments and Methods). Additional data sets were also collected on the LC8 sample containing 50 mM Cu(II)-EDTA, but due to a considerable number of chemical shift perturbations and several missing peaks, we restrict the discussion to the first sample. At the MAS frequency of 40 kHz, 10 kHz low-power TPPM (lpTPPM)[58] ^{1}H decoupling was implemented during t_1, t_2 and t_3 time periods. No proton decoupling was applied for the DCP and DREAM magnetization transfers (see Figure 1B). A 500 ms recycle delay was used (to exceed three times the ^{1}H T_1). These conditions result in a four-fold timesaving by the PACC approach using the conventional uniform Cartesian sampling. Random non-uniform sampling schedule (see Figure 2) was created by the ScheduleTool[63] based on the desired number of points, the desired maximum increment, and the estimated ^{15}N and ^{13}C T_2. This NUS schedule sampled 25% (256) hypercomplex points compared to the corresponding uniform sampling schedule (32 × 32 = 1024). Overall, the combination of PACC and NUS results in 16-fold timesaving. The total experiment times are 9 hours for NCOCA (64 scans), 14 hours for NCACO (128 scans) and 27 hours for NCACB (192 scans). We note that for LC8, conventional 3D NCOCA, NCACO and NCACB experiments are very time consuming: on our 14.1 T instrument their completion requires 6, 9 and 18 days, respectively.

As discussed above, the chemical shifts recorded in these two 3D NUS-PACC experiments, are in excellent agreement with the shifts obtained on non-doped LC8 sample using the conventional approach (see Table S2). In Figure 6, a backbone walk for the stretch of residues 21–28 is shown, generated from the 3D NUS-PACC datasets. With the NUS-PACC experiments, we corroborated the resonance assignments of LC8 established by us previously from conventional 3D MAS experiments[74]. (see Table S4) From the isotropic chemical shifts and using TALOS+, we have derived the backbone torsion angles. As shown in Figure S4, the torsion angles and the secondary structure are in excellent agreement with the previous solid-state NMR,[74] solution NMR,[49] and X-ray[75] studies.

Peak Intensities, Dynamic Range and Data Processing Methods

MaxEnt reconstruction implemented in RNMRTK seeks optimization (in an unconstrained form) of a target function that is a combination of the entropy of the reconstructed spectrum and consistency with the experimental data.[24] The relative weight of data consistency is determined by the Lagrange multiplier λ (larger λ indicates more significance is put on data

consistency). We have recently demonstrated that in the limit of high λ, full linearity of the transformation between the time and the frequency domains is attained, permitting quantitative analysis of the spectral peak intensities; we dubbed this approach MINT.[28]

In processing the NUS-PACC data sets presented here, λ was set at 5000 for NUS-NCACB, NUS-NCACO and NUS-NCOCA experiments. This is a balanced choice of λ based on the intrinsic SNR of the NMR data, and these values generally produce high-quality spectra on data with limited dynamic range. This choice of processing parameters also enabled time-efficient reconstruction of 3D spectra discussed here, without significantly compromising the absolute peak intensities as evidenced by the highly linear correlation between peak intensities in the related 2D NUS-PACC and US datasets (see Figure 7).

However, under these conditions it is possible that weak cross peaks may be overlooked in the datasets with high dynamic range.[76] Many MAS NMR experiments, especially second-order dipolar recoupling methods, cover signals with broad dynamic range. For example, this occurs in homonuclear dipolar-based correlations, where diagonal peaks are often much stronger than the associated cross peaks, and cross peak intensities vary widely depending on the magnitude of the corresponding dipolar coupling. To examine the effect of dynamic range on the MaxEnt-processed NUS spectra of LC8, we also processed two NUS-PACC NCACB and NCOCA 3D data sets acquired on LC8 doped with 50 mM Cu(II)-EDTA using MDD,[34] which has been formerly applied for data sets with broad dynamic range, such as solution NOESY data.[77,78] Spectra generated by MaxEnt and MDD are very similar, if not identical (see Figure S5). We conclude that both numerical methods are suitable for processing DCP-DREAM-based NUS-PACC data. We note that under our experimental conditions, given generally high and uniform transfer efficiency of the DREAM mixing sequence, the dynamic range of the signal is somewhat limited. If non-uniform sampling is applied in experiments aimed at collecting distance restraints where peak intensities bear critical information and long-range correlations corresponding to generally weaker peaks are valuable, it will be interesting to explore multiple data processing algorithms for a broader range of MAS NMR data sets. For example, when distance restraints are acquired under fast-MAS conditions (e.g., R2 symmetry based RDSD,[79] PARIS,[80] SHANGHAI,[72] PAR[81,82] or PAIN-CP[83]), the different signals cover broad dynamic range. We expect that in such cases data processing by methods such as MINT,[28] MDD[77] (or its variant CO-MDD[78]), or FM[35], might be advantageous for retaining weak signals.

Future Outlook

It is important to note that both the optimal ratio of sampled over omitted points and the overall sampling schedule affect the final spectral quality as well as the timesaving efficiency. In our approach, four-fold timesaving has resulted from the NUS protocol. However, it remains to be tested whether even more “aggressive” non-uniform sampling can be used in MAS SSNMR experiments. Recently, several new NUS sampling strategies that utilized probability and statistics theories were developed, and demonstrated that greater timesaving could be attained by designing advanced sampling schedules.[84]

Four-dimensional experiments were introduced by Rienstra and coworkers in the solid state several years ago.[85] However, the long experimental time required for 4D experiments has so far prevented their applications to samples of low or even moderate sensitivity. Most recently, these researchers reported the application of GFT projection NMR in MAS experiments, where they demonstrated an order-of-magnitude reduction in experiment time by jointly sampling the two indirect dimensions.[45] With this protocol, 4D spectroscopy can be carried out as (4,3)D GFT experiments. However, this approach is not suitable for samples with high intrinsic chemical shift degeneracy, such as microtubule-associated proteins LC8[74] and CAP-Gly[8] or HIV-1 CA protein assemblies[9,73] under investigation in

our laboratory. With new numerical methods available for processing data collected with NUS in three indirect dimensions, such as FM[35], msa3d of MaxEnt[84], we expect that NUS-PACC can be implemented in four-dimensional MAS NMR experiments, thus enabling site-specific resonance assignments in challenging biological systems such as protein assemblies and membrane-associated proteins.

CONCLUSIONS

We have demonstrated that simultaneous use of non-uniform sampling (NUS) and paramagnetic-relaxation-assisted condensed data collection (PACC) enables dramatic timesaving in 3D MAS NMR experiments. Specifically, we have observed 16-fold timesaving in three 3D DCP-DREAM-based experiments, NCACB, NCACO and NCOCA, which constitute the basis for the resonance assignment protocol in proteins in the solid state. The net effect is a composite of the inherent sensitivity enhancements attained due to NUS (up to two-fold in each indirect dimension) and drastic reduction in spin-lattice relaxation times permitting very short recycle delays when MAS frequencies of 40 kHz and above are used. With careful screening of the paramagnetic dopant concentration appropriate conditions can be found where the chemical shift perturbations are limited to a small number of residues at the surface of the protein. These perturbations can be corrected for by comparison of shifts with those extracted from 2D spectra of a neat non-doped protein, once the resonance assignments are established. The approach introduced here can be extended to a wide variety of 3D or 4D experiments as long as they satisfy the requirement for PACC, and is expected to be highly beneficial for structural and dynamics studies of large proteins and protein assemblies by MAS NMR, especially those possessing inherently low sensitivity.

Supplementary Material

Refer to Web version on PubMed Central for supplementary material.

Acknowledgments

This work was supported by the National Institutes of Health (NIH Grant R01GM085396 from NIGMS). Development of RNMRTK was supported in part by NIH P01-GM-047467. We thank Cheryl Arrowsmith and Aleksandras Gutmanas for providing the MDDGUI software.

REFERENCES

1. McDermott A. Annu. Rev. Biophys. 2009; 38:385–403. [PubMed: 19245337]
2. Mani R, Cady SD, Tang M, Waring AJ, Lehrer RI, Hong M. Proc. Natl. Acad. Sci U.S.A. 2006; 103:16242–16247. [PubMed: 17060626]
3. Lange A, Giller K, Hornig S, Martin-Eauclaire MF, Pongs O, Becker S, Baldus M. Nature. 2006; 440:959–962. [PubMed: 16612389]
4. Petkova AT, Yau WM, Tycko R. Biochemistry. 2006; 45:498–512. [PubMed: 16401079]
5. Chimon S, Shaibat MA, Jones CR, Calero DC, Aizezi B, Ishii Y. Nat. Struct. Mol. Biol. 2007
6. Wasmer C, Lange A, Van Melckebeke H, Siemer AB, Riek R, Meier BH. Science. 2008; 319:1523–1526. [PubMed: 18339938]
7. Helmus JJ, Surewicz K, Nadaud PS, Surewicz WK, Jaroniec CP. Proc. Natl. Acad. Sci. U.S.A. 2008; 105:6284–6289. [PubMed: 18436646]
8. Sun S, Siglin A, Williams JC, Polenova T. J. Am. Chem. Soc. 2009; 131:10113–10126. [PubMed: 19580321]
9. Han Y, Ahn J, Concel J, Byeon IJ, Gronenborn AM, Yang J, Polenova T. J. Am. Chem. Soc. 2010; 132:1976–1987. [PubMed: 20092249]

10. Wüthrich, K. NMR of proteins and nucleic acids. New York: Wiley; 1986.
11. Sattler M, Schleucher J, Griesinger C. Prog. Nucl. Magn. Reson. Spectrosc. 1999; 34:93–158.
12. Baldus M. Prog. Nucl. Magn. Reson. Spectrosc. 2002; 41:1–47.
13. Ikura M, Kay LE, Bax A. Biochemistry. 1990; 29:4659–4667. [PubMed: 2372549]
14. Grzesiek S, Dobeli H, Gentz R, Garotta G, Labhardt AM, Bax A. Biochemistry. 1992; 31:8180–8190. [PubMed: 1525157]
15. Kim S, Szyperski T. J. Am. Chem. Soc. 2003; 125:1385–1393. [PubMed: 12553842]
16. Wickramasinghe NP, Parthasarathy S, Jones CR, Bhardwaj C, Long F, Kotecha M, Mehboob S, Fung LW, Past J, Samoson A, Ishii Y. Nat. Methods. 2009; 6:215–218. [PubMed: 19198596]
17. Linser R, Chevelkov V, Diehl A, Reif B. J. Magn. Reson. 2007; 189:209–216. [PubMed: 17923428]
18. Laage S, Sachleben JR, Steuernagel S, Pierattelli R, Pintacuda G, Emsley L. J. Magn. Reson. 2009; 196:133–141. [PubMed: 19028122]
19. Bertini I, Emsley L, Lelli M, Luchinat C, Mao J, Pintacuda G. J. Am. Chem. Soc. 2010; 132:5558–5559. [PubMed: 20356036]
20. Yamamoto K, Xu J, Kawulka KE, Vederas JC, Ramamoorthy A. J. Am. Chem. Soc. 2010; 132:6929–6931. [PubMed: 20433169]
21. Nadaud PS, Helmus JJ, Sengupta I, Jaroniec CP. J. Am. Chem. Soc. 2010; 132:9561–9563. [PubMed: 20583834]
22. Kazimierczuk K, Stanek J, Zawadzka-Kazimierczuk A, Kozminski W. Prog. Nucl. Magn. Reson. Spectrosc. 2010; 57:420–434. [PubMed: 20920758]
23. Coggins BE, Venters RA, Zhou P. Prog. Nucl. Magn. Reson. Spectrosc. 2010; 57:381–419. [PubMed: 20920757]
24. Hoch JC, Stern AS. Meth. Enzymol. 2001; 338:159–178. [PubMed: 11460547]
25. Freeman R, Kupce E. J. Biomol. NMR. 2003; 27:101–113. [PubMed: 12962120]
26. Atreya HS, Szyperski T. Meth. Enzymol. 2005; 394:78–108. [PubMed: 15808218]
27. Szyperski T, Yeh DC, Sukumaran DK, Moseley HN, Montelione GT. Proc. Natl. Acad. Sci. U.S.A. 2002; 99:8009–8014. [PubMed: 12060747]
28. Paramasivam S, Suiter CL, Hou GJ, Sun SJ, Palmer M, Hoch JC, Rovnyak D, Polenova T. J. Phys. Chem. B. 2012; 116:7416–7427. [PubMed: 22667827]
29. Rovnyak D, Sarcone M, Jiang Z. Magn. Reson. Chem. 2011
30. Kupce E, Freeman R. J. Am. Chem. Soc. 2003; 125:13958–13959. [PubMed: 14611222]
31. Hiller S, Fiorito F, Wuthrich K, Wider G. Proc. Natl. Acad. Sci. U.S.A. 2005; 102:10876–10881. [PubMed: 16043707]
32. Malmodin D, Billeter M. Magn. Reson. Chem. 2006; 44:S185–S195. Spec No. [PubMed: 16823902]
33. Eghbalnia HR, Bahrami A, Tonelli M, Hallenga K, Markley JL. J. Am. Chem. Soc. 2005; 127:12528–12536. [PubMed: 16144400]
34. Jaravine V, Ibraghimov I, Orekhov VY. Nat. Methods. 2006; 3:605–607. [PubMed: 16862134]
35. Hyberts SG, Frueh DP, Arthanari H, Wagner G. J. Biomol. NMR. 2009; 45:283–294. [PubMed: 19705283]
36. Holland DJ, Bostock MJ, Gladden LF, Nietlispach D. Angew. Chem. Int. Ed. 2011; 50:6548–6551.
37. Kazimierczuk K, Orekhov VY. Angew. Chem. Int. Ed. 2011; 50:5556–5559.
38. Shrot Y, Frydman L. J. Magn. Reson. 2011; 209:352–358. [PubMed: 21316276]
39. Matsuki Y, Eddy MT, Herzfeld J. J. Am. Chem. Soc. 2009; 131:4648–4656. [PubMed: 19284727]
40. Kazimierczuk K, Kozminski W, Zhukov I. J. Magn. Reson. 2006; 179:323–328. [PubMed: 16488634]
41. Jiang B, Jiang X, Xiao N, Zhang X, Jiang L, Mao XA, Liu M. J. Magn. Reson. 2010; 204:165–168. [PubMed: 20236843]
42. Rovnyak D, Filip C, Itin B, Stern AS, Wagner G, Griffin RG, Hoch JC. J. Magn. Reson. 2003; 161:43–55. [PubMed: 12660110]

43. Jones DH, Opella SJ. J. Magn. Reson. 2006; 179:105–113. [PubMed: 16343957]
44. Matsuki Y, Eddy MT, Griffin RG, Herzfeld J. Angew. Chem. Int. Ed. Engl. 2010
45. Franks WT, Atreya HS, Szyperski T, Rienstra CM. J. Biomol. NMR. 2010
46. Maly T, Debelouchina GT, Bajaj VS, Hu KN, Joo CG, Mak-Jurkauskas ML, Sirigiri JR, van der Wel PC, Herzfeld J, Temkin RJ, Griffin RG. J. Chem. Phys. 2008; 128:052211. [PubMed: 18266416]
47. Duma L, Hediger S, Brutscher B, Bockmann A, Emsley L. J. Am. Chem. Soc. 2003; 125:11816–11817. [PubMed: 14505393]
48. Laage S, Lesage A, Emsley L, Bertini I, Felli IC, Pierattelli R, Pintacuda G. J. Am. Chem. Soc. 2009; 131:10816–10817. [PubMed: 19722659]
49. Lightcap CM, Sun S, Lear JD, Rodeck U, Polenova T, Williams JC. J. Biol. Chem. 2008; 283:27314–27324. [PubMed: 18650427]
50. Marulanda D, Tasayco ML, McDermott A, Cataldi M, Arriaran V, Polenova T. J. Am. Chem. Soc. 2004; 126:16608–16620. [PubMed: 15600367]
51. Neue G, Dybowski C. Solid State Nucl. Magn. Reson. 1997; 7:333–336. [PubMed: 9176939]
52. Thurber KR, Tycko R. J. Magn. Reson. 2009; 196:84–87. [PubMed: 18930418]
53. Morcombe CR, Zilm KW. J. Magn. Reson. 2003; 162:479–486. [PubMed: 12810033]
54. Levitt, MH. Spin dynamics : basics of nuclear magnetic resonance. Chichester; New York: John Wiley & Sons; 2001.
55. Schaefer J, McKay RA, Stejskal EO. J. Magn. Reson. 1979; 34:443–447.
56. Baldus M, Petkova AT, Herzfeld J, Griffin RG. Mol. Phys. 1998; 95:1197–1207.
57. Bennett AE, Rienstra CM, Auger M, Lakshmi KV, Griffin RG. J. Chem. Phys. 1995; 103:6951–6958.
58. Kotecha M, Wickramasinghe NP, Ishii Y. Magn. Reson. Chem. 2007; 45:S221–S230.
59. Bennett AE, Rienstra CM, Griffiths JM, Zhen W, Lansbury PT, Griffin RG. J. Chem. Phys. 1998; 108:9463–9479.
60. Ishii Y. J. Chem. Phys. 2001; 114:8473–8483.
61. Verel R, Baldus M, Ernst M, Meier BH. Chem. Phys. Lett. 1998; 287:421–428.
62. States DJ, Haberkorn RA, Ruben DJ. J. Magn. Reson. 1982; 48:286–292.
63. Maciejewski, MW.; Gorbatyuk, V.; Hoch, JC. ScheduleTool.
64. Wishart DS, Bigam CG, Yao J, Abildgaard F, Dyson HJ, Oldfield E, Markley JL, Sykes BD. J. Biomol. NMR. 1995; 6:135–140. [PubMed: 8589602]
65. Delaglio F, Grzesiek S, Vuister GW, Zhu G, Pfeifer J, Bax A. J. Biomol. NMR. 1995; 6:277–293. [PubMed: 8520220]
66. Hoch, JC.; Stern, AS. NMR Data Processing. New York: Wiley-Liss; 1996.
67. Stern AS, Li KB, Hoch JC. J. Am. Chem. Soc. 2002; 124:1982–1993. [PubMed: 11866612]
68. Mobli M, Maciejewski MW, Gryk MR, Hoch JC. J. Biomol. NMR. 2007; 39:133–139. [PubMed: 17701276]
69. Goddard, TD.; Kneller, DG. Sparky 3.
70. McConnell HM, Robertson RE. J. Chem. Phys. 1958; 29:1361–1365.
71. Shen M, Hu B, Lafon O, Trebosc J, Chen Q, Amoureux JP. J. Magn. Reson. 2012; 223:107–119. [PubMed: 22985981]
72. Hu B, Lafon O, Trebosc J, Chen Q, Amoureux J-P. J. Magn. Reson. 2011; 212:320–329. [PubMed: 21873091]
73. Byeon IJL, Hou GJ, Han Y, Suiter CL, Ahn J, Jung J, Byeon CH, Gronenborn AM, Polenova T. J. Am. Chem. Soc. 2012; 134:6455–6466. [PubMed: 22428579]
74. Sun S, Butterworth AH, Paramasivam S, Yan S, Lightcap CM, Williams JC, Polenova T. Can. J. Chem. 2011; 89:909–918.
75. Williams JC, Roulhac PL, Roy AG, Vallee RB, Fitzgerald MC, Hendrickson WA. Proc. Natl. Acad. Sci. U.S.A. 2007; 104:10028–10033. [PubMed: 17551010]

76. Hyberts SG, Heffron GJ, Tarragona NG, Solanky K, Edmonds KA, Luithardt H, Fejzo J, Chorev M, Aktas H, Colson K, Falchuk KH, Halperin JA, Wagner G. J. Am. Chem. Soc. 2007; 129:5108–5116. [PubMed: 17388596]
77. Tugarinov V, Kay LE, Ibraghimov I, Orekhov VY. J. Am. Chem. Soc. 2005; 127:2767–2775. [PubMed: 15725035]
78. Hiller S, Ibraghimov I, Wagner G, Orekhov VY. J. Am. Chem. Soc. 2009; 131:12970–12978. [PubMed: 19737017]
79. Hou G, Yan S, Sun S, Han Y, Byeon IJ, Ahn J, Concel J, Samoson A, Gronenborn AM, Polenova T. J. Am. Chem. Soc. 2010
80. Weingarth M, Demco DE, Bodenhausen G, Tekely P. Chem. Phys. Lett. 2009; 469:342–348.
81. De Paepe G, Lewandowski JR, Loquet A, Bockmann A, Griffin RG. J. Chem. Phys. 2008; 129:245101. [PubMed: 19123534]
82. Lewandowski JR, De Paepe G, Eddy MT, Struppe J, Maas W, Griffin RG. J. Phys. Chem. B. 2009; 113:9062–9069. [PubMed: 19489532]
83. Lewandowski JR, De Paepe G, Griffin RG. J. Am. Chem. Soc. 2007; 129:728–729. [PubMed: 17243786]
84. Mobli M, Stern AS, Bermel W, King GF, Hoch JC. J. Magn. Reson. 2010; 204:160–164. [PubMed: 20299257]
85. Franks WT, Kloepper KD, Wylie BJ, Rienstra CM. J. Biomol. NMR. 2007; 39:107–131. [PubMed: 17687624]

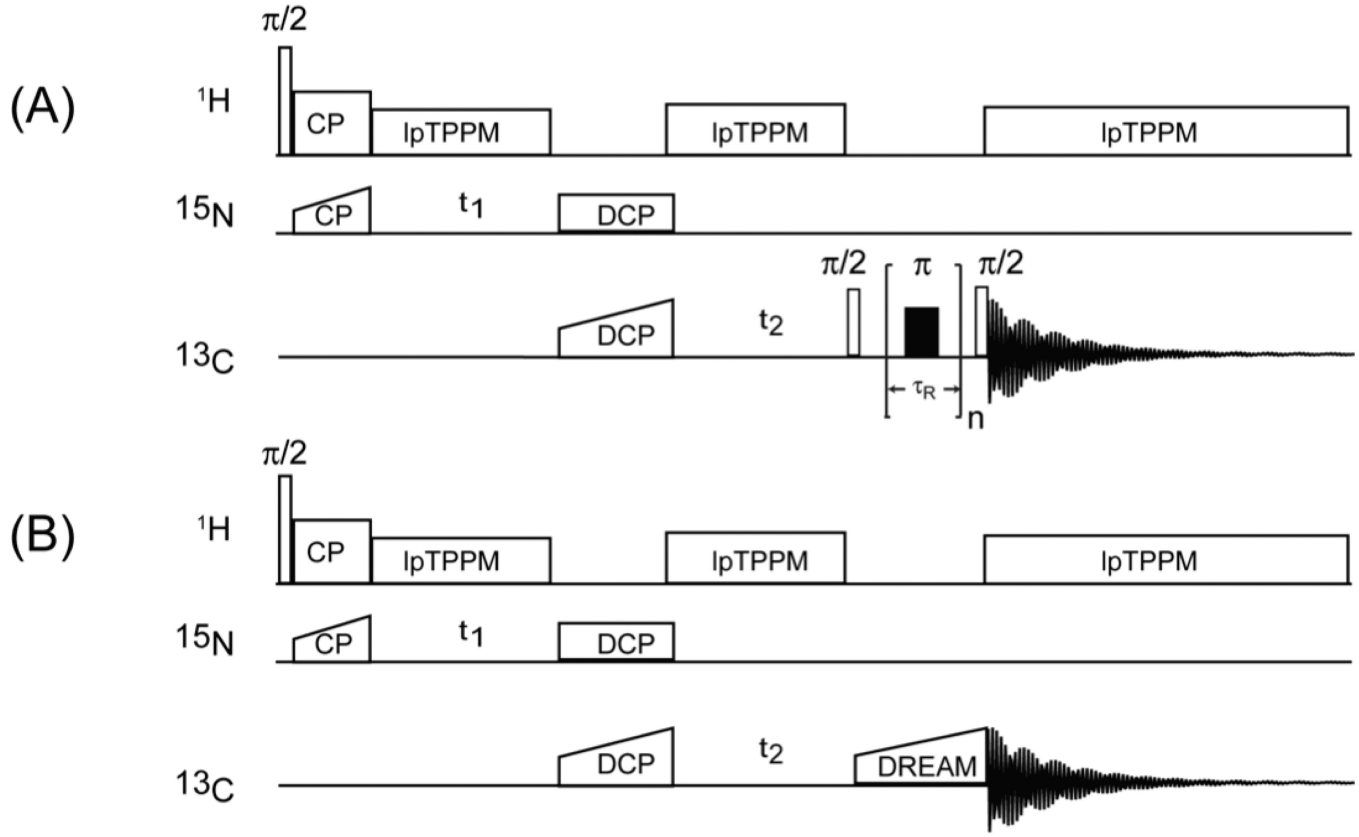

Figure 1.
Pulse sequences for NUS-PACC experiments: (A) DCP-RFDR pulse sequence for NCOCX and NCACX 3D experiments; (B) DCP-DREAM pulse sequence for NCOCA, NCACO and NCACB 3D experiments.

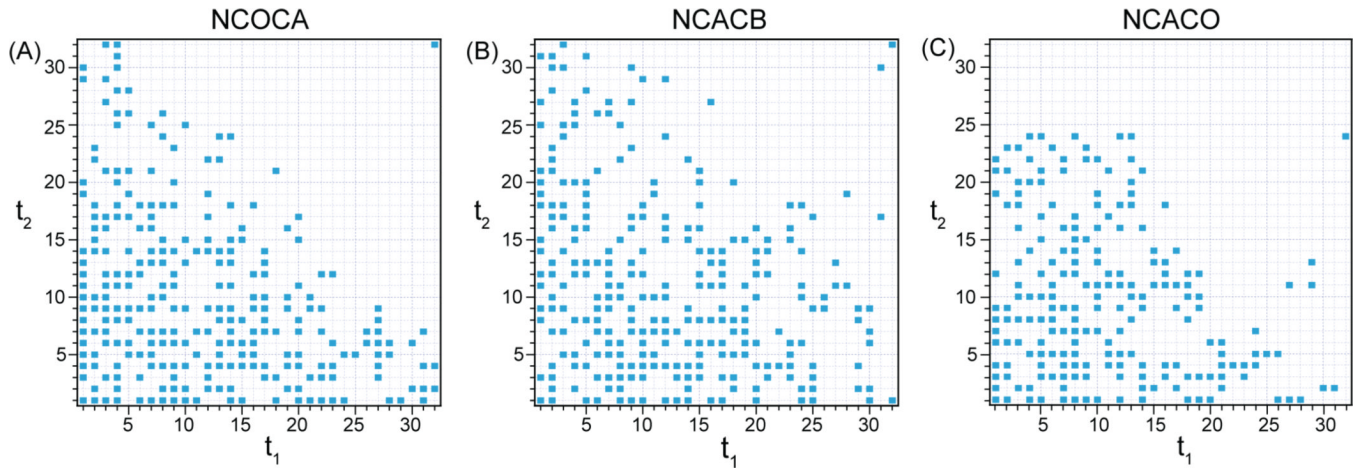

Figure 2.

Sampling schedule for NUS-PACC 3D (A) NCOCA, (B) NCACB and (C) NCACO experiments for the 5 mM Cu(II)-EDTA sample. Each point represents four FIDs combined from the real (R) and imaginary (I) parts in the order of (t_1, t_2): RR, IR, RI, II. For the sampling schedules of NCOCA and NCACB experiments, 25% points of a 32×32 uniform sampling schedules were used. For the sampling schedule of the NCACO experiment, 25% points of a 32 × 24 uniform sampling schedule was used.

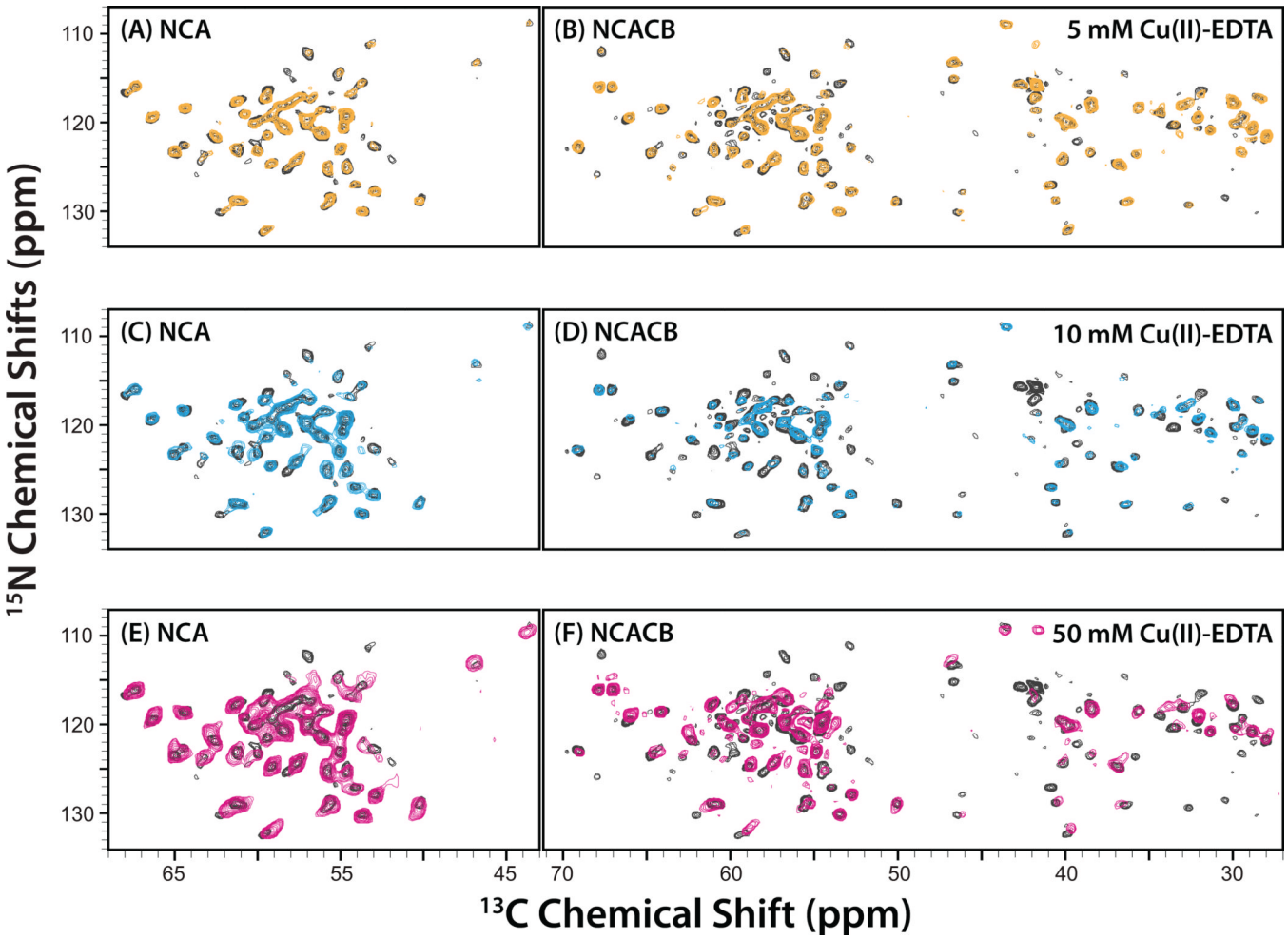

Figure 3.
2D NCA (left) and NCACB (right) spectra of U-^{13}C,^{15}N-LC8 doped with 5 mM (top, yellow), 10 mM (middle, blue), and 50 mM (bottom, magenta) Cu(II)-EDTA, overlaid onto the corresponding spectra of the neat protein sample (black).

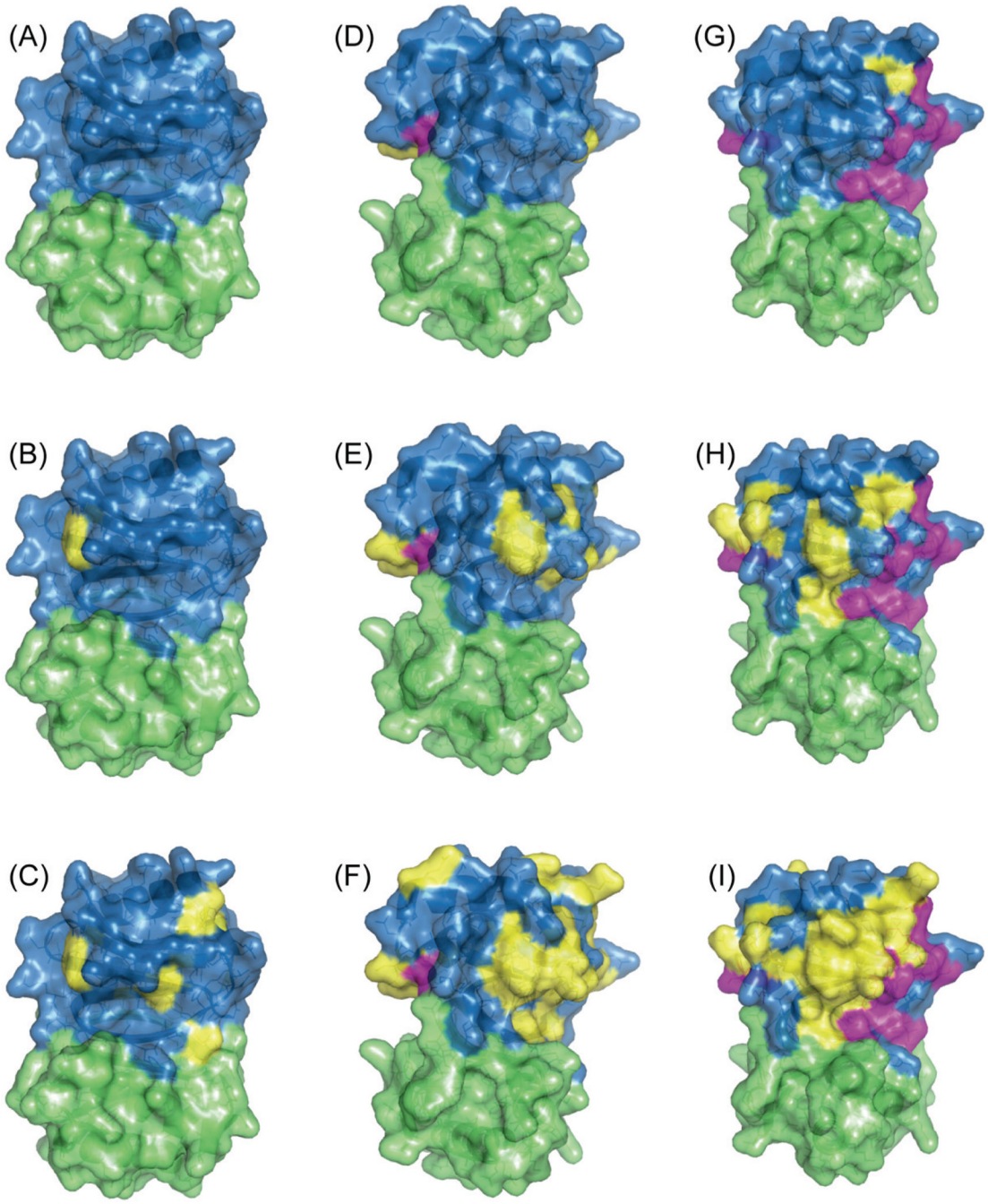

Figure 4.

Surface representation of the X-ray structure of LC8 (2PG1[75]) depicting the residues either missing (in magenta) or with perturbed peaks (in yellow) in 3D NCACB spectra of samples doped with different concentration of Cu(II)-EDTA: 5 mM (left column), 10 mM (middle column), and 50 mM (right column). The two monomers of LC8 are shown in blue and green. The top, middle and bottom rows present the residues with perturbations larger than 0.5 ppm, 0.2 ppm, and 0.1 ppm for ^{13}C, respectively.

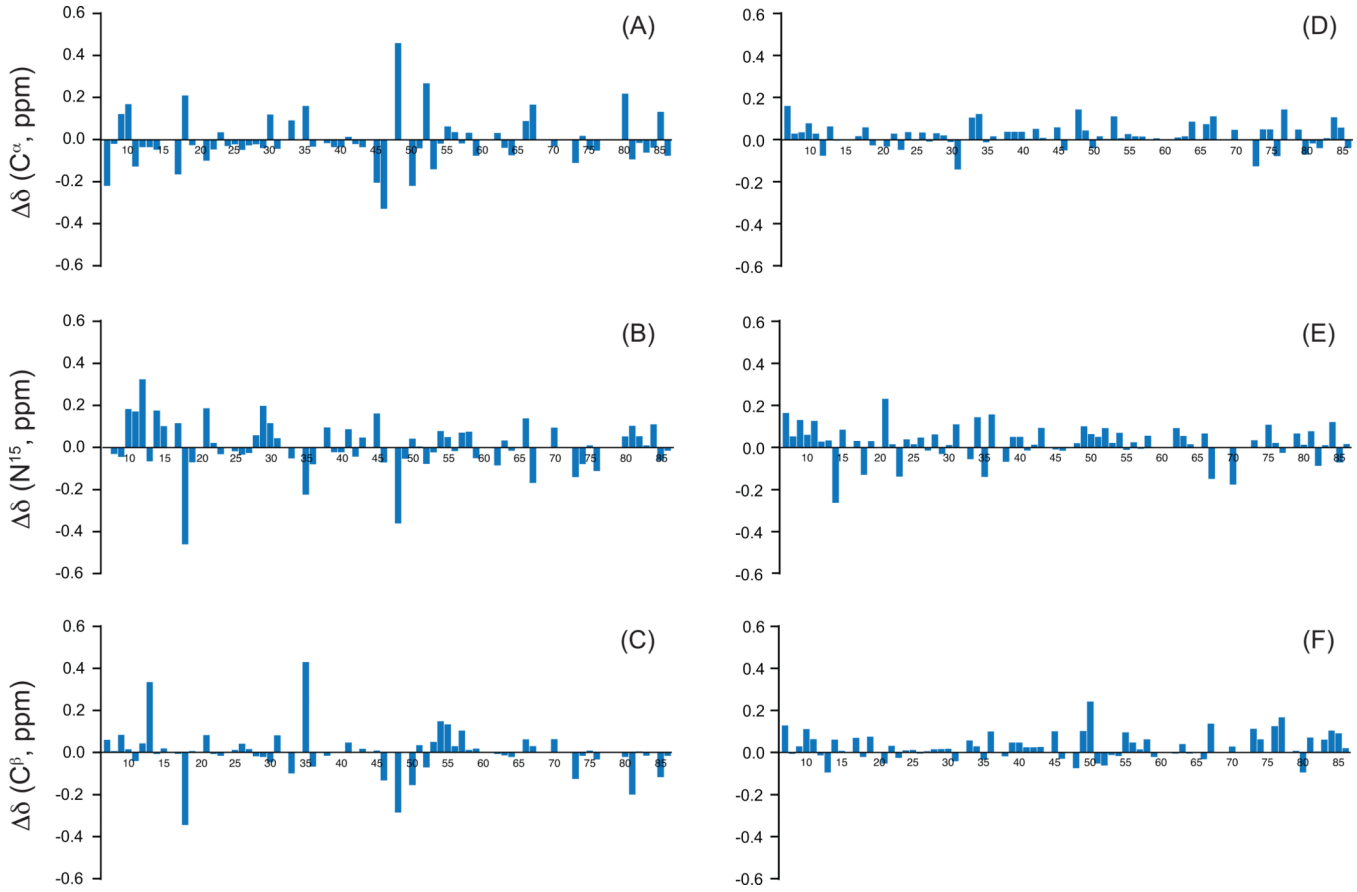

Figure 5.

Chemical shift differences plotted for each residue in the LC8 sample doped with 5 mM Cu(II)-EDTA, for the following atom types: $^{13}C_a$ (A, D), ^{15}N (B, E), and $^{13}C_b$ (C, F). The left panel (A–C) is the difference of chemical shifts between two 3D NCACB uniformly sampled spectra. The right panel (D–F) is the difference of chemical shifts between two 3D NCACB spectra, one acquired by non-uniform sampling in both indirect dimensions and another- by uniform sampling. The US spectrum used as the reference dataset in both the left and right panel was acquired as a 32×32 point hypercomplex matrix in two indirect dimensions; the total evolution time is 12.4 ms and 6.9 ms in the indirect ^{15}N (t_1) and ^{13}C (t_2) dimensions, respectively. The second US data used for chemical shift comparison has shorter evolution time in N and CA dimensions (50% of evolution time in N dimension, and 37.5% of evolution time in CA dimension). The NUS spectrum was acquired using a 3D NUS schedule consisting of 25% points of the corresponding reference US dataset and using the same spectral width and the same evolution time in all dimensions. Note that the chemical shift differences between the NUS and US spectra are small and below 0.2 ppm for the overwhelming majority of the residues. On the other hand, the two US spectra exhibit significantly higher chemical shift deviations.

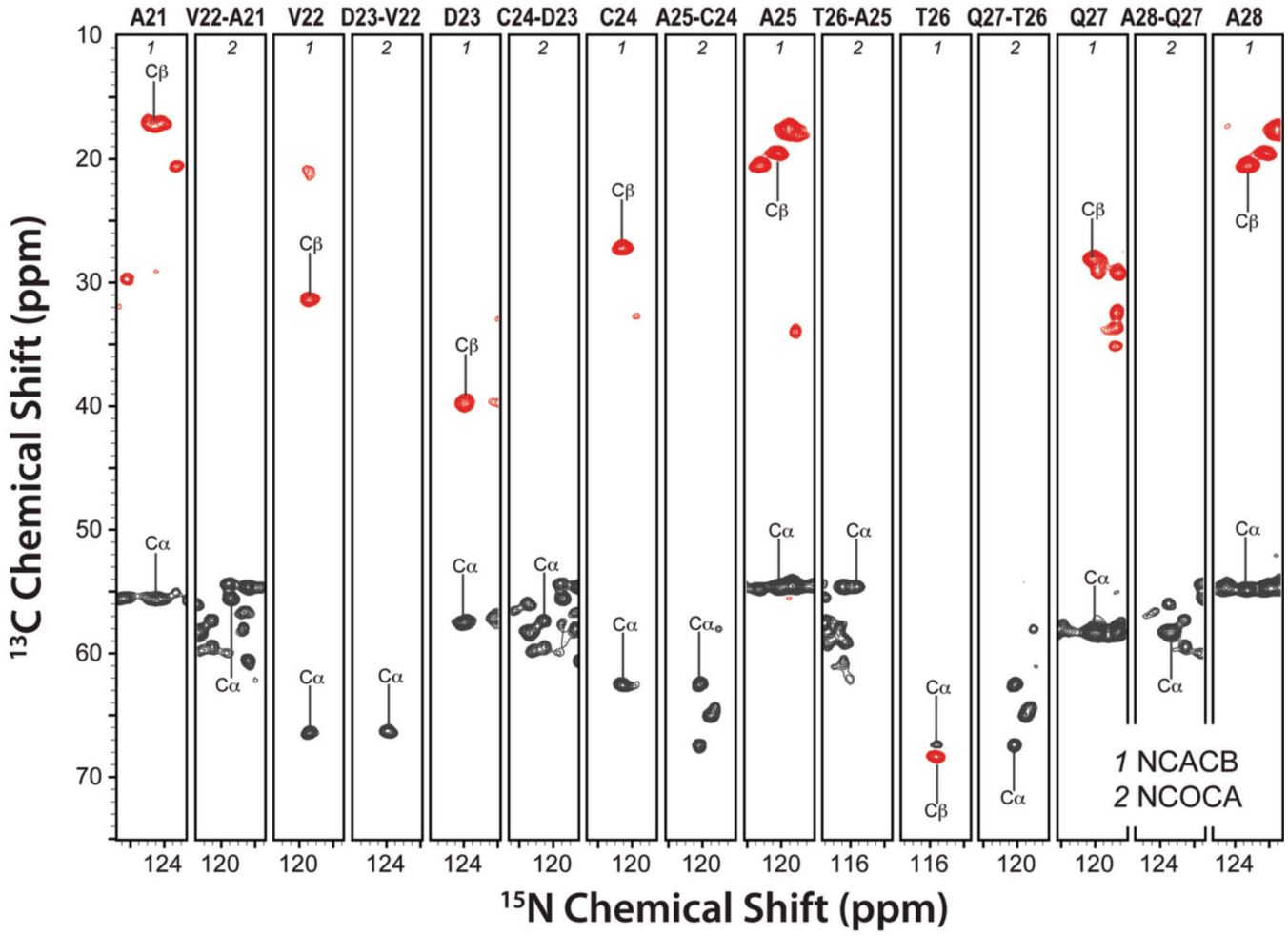

Figure 6.

Backbone walk for A21–A28 using three-dimensional NUS-PACC experiments: DCP-DREAM based NCACB and NCOCA. Acquisition and processing parameters for each experiment are presented in the Experiments and Methods.

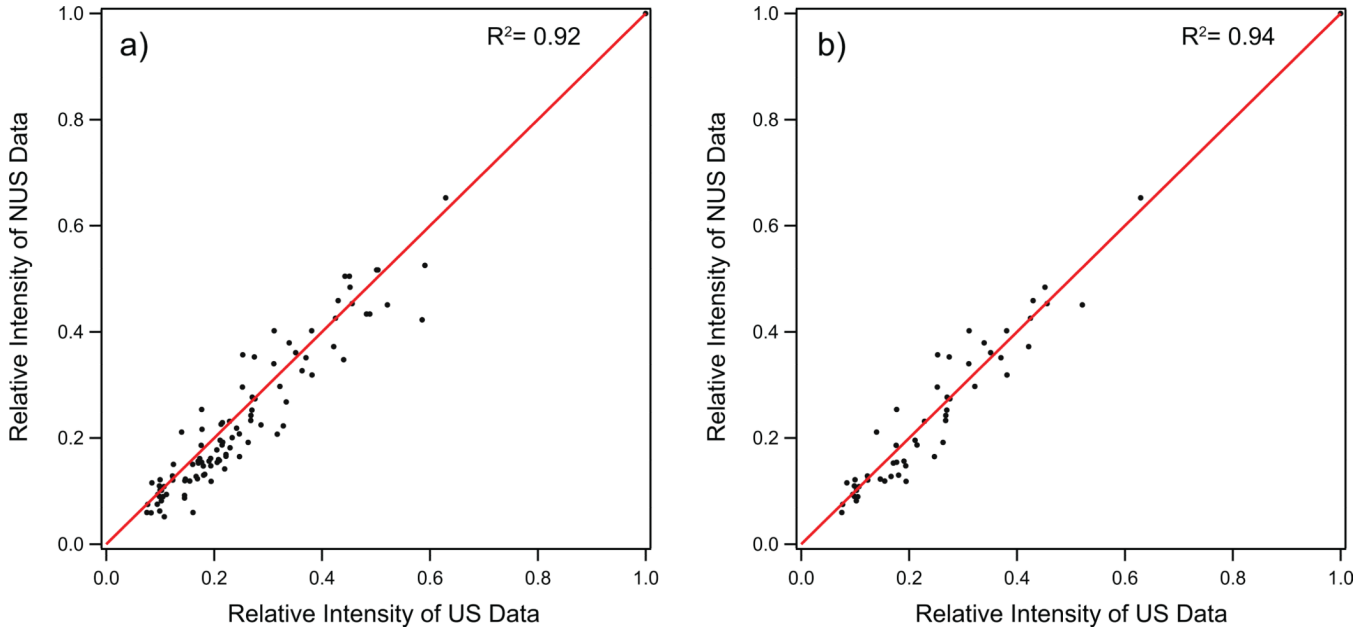

Figure 7.

The correlation plot of relative peak intensity of 2D NCACB NUS spectrum vs US spectrum. (a) The correlations including diagonal-peaks (N-CA-CA) and cross-peaks (N-CA-CB) for 2D NUS vs 2D US. (b) The correlation plot of cross-peaks (N-CA-CB) only. Both spectra were processed by RNMRTK with high λ (following MINT protocol).

Table 1

Dopant Concentration Dependencies of ^{1}H T_1 and ^{15}N T_2 for LC8.

MAS frequency	Cu(II) –EDTA concentrations	^{1}H T_1 (ms)	^{15}N T_2 (ms)
10 kHz	0 mM	422 ± 8	23 ± 1
	10 mM	82 ± 3	Not measured
	20 mM	83 ± 3	Not measured
	50 mM	48 ± 1	29 ± 2
40 kHz	0 mM	632 ± 7	24 ± 2
	5 mM	151 ± 2	21 ± 2
	10 mM	115 ± 2	17 ± 2
	50 mM	73 ± 3	26 ± 1

Experiments at 40 kHz MAS were conducted on a U-^{15}N, ^{13}C labeled LC8, experiments at 10 kHz MAS frequency were conducted on a U-^{15}N labeled LC8.

Table 2

Signal-to-Noise Ratio of 1D DCP-RFDR and DCP-DREAM Spectra Recorded in 50 mM Cu(II)-EDTA Doped U-^{13}C, ^{15}N-Labeled LC8 Sample.

	DCP-RFDR		DCP-DREAM		
S/N*	NCACX (256 scans)	NCOCX (64 scans)	NCACB (256 scans)	NCACO (256 scans)	NCOCA (64 scans)
C'	11.8	21.3	-	20.2	22.2
C^a	6.6	4.6	9.7	11.9	8.6
C^b	3.2	-	8.4	-	-

*The signal to noise ratio at different regions are measured for the tallest peak in each region.